
QuantFace: Low-Bit Post-Training Quantization for One-Step Diffusion Face Restoration

Jiatong Li^{1*}, Libo Zhu^{1*}, Haotong Qin², Jingkai Wang¹, Linghe Kong^{1†},
 Guihai Chen¹, Yulun Zhang^{1†}, Xiaokang Yang¹

¹Shanghai Jiao Tong University,

²ETH Zürich

Abstract

Diffusion models have been achieving remarkable performance in face restoration. However, the heavy computations of diffusion models make it difficult to deploy them on devices like smartphones. In this work, we propose QuantFace, a novel low-bit quantization for one-step diffusion face restoration models, where the full-precision (*i.e.*, 32-bit) weights and activations are quantized to 4~6-bit. We first analyze the data distribution within activations and find that they are highly variant. To preserve the original data information, we employ rotation-scaling channel balancing. Furthermore, we propose Quantization-Distillation Low-Rank Adaptation (QD-LoRA) that jointly optimizes for quantization and distillation performance. Finally, we propose an adaptive bit-width allocation strategy. We formulate such a strategy as an integer programming problem, which combines quantization error and perceptual metrics to find a satisfactory resource allocation. Extensive experiments on the synthetic and real-world datasets demonstrate the effectiveness of QuantFace under 6-bit and 4-bit. QuantFace achieves significant advantages over recent leading low-bit quantization methods for face restoration. The code is available at <https://github.com/jiatongli2024/QuantFace>.

1 Introduction

Face restoration seeks to recover high-quality (HQ) facial images from degraded low-quality (LQ) inputs. The LQ inputs are generated from complex degradation processes, such as blurring, noise, downsampling, and JPEG compression. With the rapid development of deep generative models, generative adversarial networks (GANs) [1] and diffusion-based methods [2, 3, 4] have attracted increasing attention. Several approaches [5, 6, 7, 8] have already demonstrated impressive capability in restoring HQ human faces. Nevertheless, GANs typically suffer from training instability due to adversarial learning, while multi-step diffusion models demand extensive computational resources.

To accelerate inference, recent studies have proposed one-step diffusion (OSD) [9, 10, 11] schemes that reduce the denoising step to one. At the same time, these models largely preserve the performance of the original multi-step diffusion models. Thanks to these advanced techniques, one-step diffusion face restoration (OSDFR) models [12] have become feasible. However, despite this progress, deploying such models on resource-constrained platforms (*e.g.*, smartphones or other mobile devices) remains challenging, because they still require prohibitive computational resources. This limitation hinders the widespread adoption of diffusion-based face restoration methods in real-world scenarios.

Model quantization [16] offers an effective avenue to further accelerate OSDFR models. By mapping both weights and activations from full-precision (FP) to low-bit precision, quantization significantly

*Equal contribution.

†Corresponding authors: Yulun Zhang, yulun100@gmail.com; Linghe Kong, linghe.kong@sjtu.edu.cn



	LQ	DiffBIR [13]	OSDFace [12]	PassionSR [14]	SVDQuant [15]	QuantFace (ours)
# Step / Bits		50 / W32A32	1 / W32A32	1 / W4A4	1 / W4A4	1 / W4A4
Param. (M) / Ops (G)		1,618 / 49,056	978 / 4,264	122 / 533	148 / 728	148 / 728

Figure 1: Visual comparison between the multi-step diffusion and one-step diffusion face restoration models in full-precision, recent quantization methods in 4-bit, and our QuantFace in 4-bit. Our method achieves an 84.85% parameter compression and an 82.91% speedup compared with the full-precision OSDFace [12].

reduces memory footprint and computational overhead. Nevertheless, the performance gap between the quantized and the FP version is inevitable, especially under the aggressive 4-bit setting. Minimizing this gap is therefore vital for the successful implementation of quantized OSDFR models. Although current low-bit quantization strategies have achieved promising results for multi-step diffusion models and for text-to-image generation [17, 18, 19, 15, 20, 21], significant performance drops occur when we apply these methods to OSDFR models. There are three main challenges in low-bit quantization for OSDFR. **First**, the distribution of dynamic activation values is poorly preserved by static quantizers. **Second**, current distillation schemes from full-precision (FP) to quantized models are suboptimal. **Third**, the limited computational resources are not properly allocated. In this work, we propose QuantFace, a unified and effective low-bit quantization framework for OSDFR models. We select OSDFace [12] as our quantization backbone due to its excellent performance. To address the aforementioned challenges, we propose tailored solutions for each. **First**, we conduct a detailed analysis of the activation distributions in OSDFace and find that different channels of the activation values exhibit high variance. Previous scaling based methods [22, 15] can remove the outliers from activations to weights and thus decrease quantization error. However, these methods are ineffective in preserving the original activation distribution after per-tensor quantization. We find that the distribution information is vital for basic facial structure generation. To solve the problem, we propose rotation-scaling channel balancing. We consider rotation and scaling simultaneously to maintain a uniform activation distribution. **Second**, to promote alignment between the FP model and the quantized model, we propose Quantization-Distillation Low-Rank Adaptation (QD-LoRA). QD-LoRA effectively compensates for quantization error while facilitating distillation between the FP model and the quantized model. **Third**, we propose adaptive bit-width allocation. We analyze the layer-wise sensitivity to quantization and configure the bottlenecks. We design an integer programming-based algorithm for mixed-precision activation configuration. This algorithm incorporates perceptual metrics and numeric reconstruction error as the optimization target and promotes reasonable resource allocation.

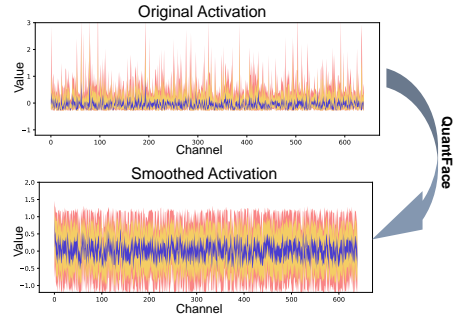


Figure 2: The original activation has high variance. Our QuantFace can smooth activation distribution and reduce quantization error.

We have conducted extensive evaluations on both synthetic and real-world datasets. As shown in Fig. 1, under 4-bit quantization, our method achieves a significant speedup compared to the multi-step face restoration model DiffBIR [13] while preserving comparable visual quality. Furthermore, Tab. 2 demonstrates that at 4-bit precision, we attain parameter and computational cost compression ratios of 84.85% and 82.91%, respectively, compared with OSDFace [12]. These findings validate the efficacy of our proposed approaches for quantizing OSDFR models.

In summary, our contributions are as follows:

- We conduct a detailed analysis of the activation distribution of the OSDFR model and identify that quantization of activation values is crucial for preserving facial features. We configure that the inadequate processing of highly variant activations is the key reason for the performance degradation in quantization.
- We propose QuantFace, a unified quantization framework for OSDFR models. It consists of rotation-scaling channel balancing, QD-LoRA, and adaptive bit-width allocation.

- Our rotation-scaling channel balancing strategy effectively preserves the original activation information, while QD-LoRA enhances the alignment between the quantized model and FP model. Meanwhile, adaptive bit-width allocation facilitates reasonable usage of resources.
- Extensive experiments on the synthetic and real-world datasets demonstrate the superior performance of our method. Quantitative and qualitative results show that our method significantly outperforms existing quantization approaches. Under the extreme 4-bit setting, our model is still capable of generating high-quality face images.

2 Related Works

2.1 Face Restoration

Face restoration seeks to reconstruct high-fidelity facial images from degraded low-quality inputs affected by diverse and complex distortions. A central challenge in this domain is how to incorporate facial priors efficiently and effectively. While classical methods have long leveraged statistical priors, recent advances in deep generative techniques (such as GANs [1] and diffusion models [2, 3, 23]) have driven growing interest in generative priors.

In particular, diffusion-based priors [5, 6, 7, 8] have attracted considerable attention. These methods generate HQ images by gradually removing noise from LQ inputs. Concurrently, vector-quantized (VQ) prior approaches [24, 25, 26, 27] are promising. They map LQ features to discrete codebook entries and then decode the HQ images from the codebook.

The combination of VQ priors and generative diffusion priors has become very popular recently. However, while these hybrid methods can generate excellent human face images, the computational demands become severe. Consequently, developing efficient and effective compression techniques for these models has become a major focus of current research.

2.2 Model Quantization

Model quantization improves computational efficiency by reducing the precision of model parameters while maintaining performance. Quantization methods are broadly classified into two categories based on whether weight retraining is involved: post-training quantization (PTQ) [28, 29] and quantization-aware training (QAT) [30, 31, 32]. Furthermore, quantization has been demonstrated as an effective technique for compressing large language models (LLMs) [33, 34, 35, 22] for deployment on edge devices. With the rapid advancements in diffusion models (DMs), there has been a growing focus on enhancing their efficiency through quantization techniques including PTQ methods such as PTQ4DM [19], Q-Diffusion [36], and PTQD [18], as well as QAT methods like Q-DM [37]. Recently, EfficientDM [21] introduced a low-rank quantization fine-tuning strategy, while SVDQuant [15] employs 16-bit parallel low-rank branches to preserve performance. PassionSR [14] presents an innovative quantization strategy, achieving 8-bit and 6-bit quantization for one-step diffusion-based super-resolution (OSDSR) models. However, research on the quantization of OSDFR models remains limited, despite their significant differences from traditional DMs.

3 Methods

3.1 Preliminaries

Diffusion Model. Diffusion models [23] employ a two-stage procedure. First, a complex data distribution is gradually corrupted by successive injections of Gaussian noise. Second, a neural network learns the inverse of this noising process to restore the original samples. In the forward diffusion, the original sample \mathbf{x}_0 is progressively transformed into pure Gaussian noise \mathbf{x}_T by injecting random noise over T steps, formally defined as [3]:

$$\mathbf{x}_t = \sqrt{\bar{\alpha}_t} \mathbf{x}_0 + \sqrt{1 - \bar{\alpha}_t} \epsilon, \quad \epsilon \sim \mathcal{N}(0, \mathbf{I}), \quad (1)$$

where $\bar{\alpha}_t$ is a scheduling parameter, and t denotes the time step.

After T iterations, the data pattern converges to a standard Gaussian distribution: $\mathbf{x}_T \sim \mathcal{N}(0, \mathbf{I})$. Reversed diffusion process reconstructs the original distribution by predicting the noise $\epsilon_\theta(\mathbf{x}_t, t)$ formulated as follows [3]:

$$\mathbf{x}_{t-1} = \sqrt{\bar{\alpha}_{t-1}} \left(\frac{\mathbf{x}_t - \sqrt{1 - \bar{\alpha}_t} \epsilon_\theta(\mathbf{x}_t, t)}{\sqrt{\bar{\alpha}_t}} \right) + \sqrt{1 - \bar{\alpha}_{t-1} - \sigma_t^2} \cdot \epsilon_\theta(\mathbf{x}_t, t) + \sigma_t \epsilon_t, \quad (2)$$

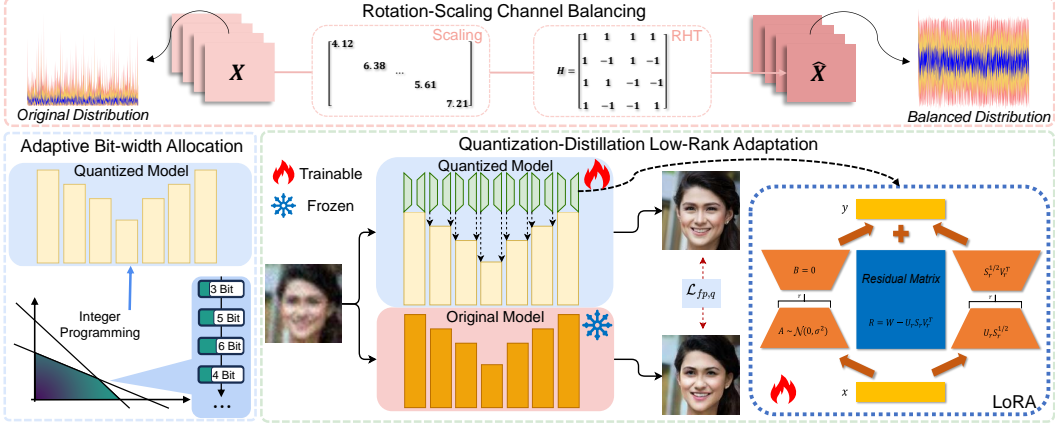


Figure 3: Overview of our QuantFace. **First**, under the 4-bit precision setting, we use the quantization errors and perceptual importance weights as the objective for integer programming, and allocate appropriate precision to activation of each layer. **Second**, before training, we integrate the scaling factor and rotation matrix into the weights, and only apply an online Randomized Hadamard Transform in the convolution layers. **Third**, we align the quantized model with the FP model on the calibration dataset by optimizing the dual-branch low-rank matrices we design.

where $\epsilon_\theta(\mathbf{x}_t, t)$ represents the output of the noise prediction network, σ_t^2 denotes the noise variance at step t , and ϵ_t is random noise irrelevant to \mathbf{x}_t . By gradually predicting the random noise at timestep t , the model progressively optimizes \mathbf{x}_t to \mathbf{x}_0 , and ultimately generates high-quality samples. Our one-step estimation can be formulated as [9]:

$$\mathbf{x}_0 \approx \frac{\mathbf{x}_t - \sqrt{1 - \bar{\alpha}_t} \epsilon_\theta(\mathbf{x}_t, t)}{\sqrt{\bar{\alpha}_t}} \quad (3)$$

Model Quantization. Model quantization [38] is an effective alternative to reduce memory and computational costs by converting floating-point numbers to fixed-point numbers. This process utilizes approximation with integer x_{int} and quantization parameters (scaling factor s , zero point z). The fake quantization process can be defined as [16]:

$$x_{\text{int}} = \text{clamp} \left(\left\lfloor \frac{\mathbf{x}}{s} \right\rfloor - z, l, u \right), \hat{x} = s \cdot x_{\text{int}} + z, \quad (4)$$

where x_{int} refers to the quantized integer and \hat{x} is the simulated quantized float-point number. $\lfloor \cdot \rfloor$ is the round-to-nearest operator, and $\text{clamp}(\cdot, l, u)$ ensures values remain within the range $[l, u]$.

To address the non-differentiability of the rounding operation, we employ the straight-through estimator (STE [39]) to approximate the gradients during backpropagation:

$$\frac{\partial Q(x)}{\partial x} \approx \begin{cases} 1 & \text{if } x \in [l, u], \\ 0 & \text{otherwise.} \end{cases} \quad (5)$$

3.2 Rotation-Scaling Channel Balancing

In any quantization method, appropriately managing the relationship between outliers and non-outliers is of critical importance. Existing channel-scaling methods can shift the quantization difficulty from activations to weights [15, 22]. After scaling, activations exhibit reduced magnitude and fewer outliers, resulting in lower quantization error. However, when it comes to convolution neural networks like Unet [40], we typically employ per-tensor quantization for activations, which means a single set of quantization parameters is shared across all channels of a tensor. Although the aforementioned scaling method suppresses extreme outliers, inter-channel imbalance still remains. When the bit-width is extremely low (e.g., 4-bit), the performance of the quantized model drops significantly.

To solve the problem, incoherent processing via Randomized Hadamard Transform (RHT) has recently emerged as a promising technique [41], and it has been shown to be a remarkable quantization method for LLMs [42, 43] and ViTs [44]. This approach requires no parameter tuning and can effectively generate a uniform data distribution across channels, thereby maximally preserving information after quantization. However, this method cannot adequately smooth extreme outliers.

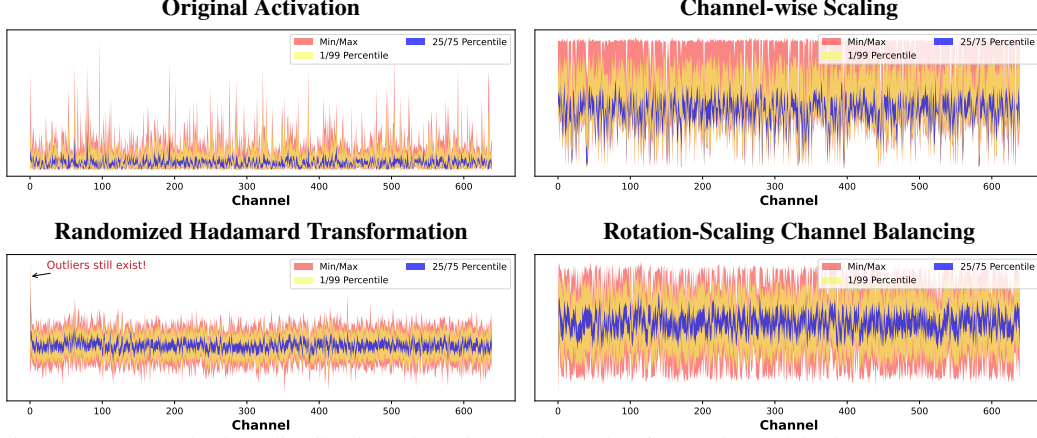


Figure 4: A sample data distribution along input channels of unet.down_blocks.1.resnets.1.conv2 activations. They are processed with different balancing techniques. Directly employing the Scaling or Randomized Hadamard Transformation will not result in satisfactory distribution for quantization.

To overcome these limitations, we propose rotation-scaling channel balancing. We find that simultaneously considering scaling and rotation techniques can reduce quantization error effectively. And this method maximally preserves the distribution information of the original data. Figure 4 illustrates the efficacy after applying the rotation-scaling channel balancing.

To the best of our knowledge, prior quantization works primarily focused on Transformer architectures. We are the first to design a scaling and rotation channel balancing method for convolution neural networks like UNet [40]. Through our analysis, we show that convolution can be transformed to matrix multiplication to some degree. The original 2D-convolution can be written as:

$$y_{f,i,j} = \sum_{u=1}^{K_w} \sum_{v=1}^{K_h} \sum_{c=1}^C k_{f,c,u,v} x_{c,i+u-1,j+v-1} = \sum_{u=1}^{K_w} \sum_{v=1}^{K_h} \mathbf{k}_{f,u,v}^T \mathbf{x}_{i+u-1,j+v-1}, \quad (6)$$

where C, K_w, k_h represents the number of input channels, kernel width, and kernel height. $\mathbf{k}_{f,u,v}, \mathbf{x}_{h+u-1,w+v-1}$ are tensors with C elements. For simplicity, let:

$$\mathbf{k}_{f,u,v} \triangleq \mathbf{k} \in \mathbb{R}^C, \mathbf{x}_{h+u-1,w+v-1} \triangleq \mathbf{x} \in \mathbb{R}^C, \quad (7)$$

so we have:

$$\mathbf{k}^T \mathbf{x} = (\mathbf{k}^T \odot s) \left(\frac{1}{s} \odot \mathbf{x} \right) = \mathbf{k}^T \mathbf{H}^T \mathbf{H} \mathbf{x}, \quad s = \frac{\max_{(h,w)} (|\mathbf{X}|)^\alpha}{\max_{(C,K_w,K_h)} (|\mathbf{K}|)^{1-\alpha}}, \quad (8)$$

where $\mathbf{K} \in \mathbb{R}^{F \times C \times K_w \times K_h}$, $\mathbf{X} \in \mathbb{R}^{C \times h \times w}$ is convolution kernel and input tensor of the layer. \mathbf{H} is a Hadamard matrix. We find that for convolution layers in OSDFace [12], the corresponding Hadamard matrices exist. According to [41], only a minimal amount of memory is required to store the corresponding random ± 1 vector of each matrix. To minimize the additional computational overhead, inspired by the offline transformation strategies from [42, 45], we integrate most of the scaling factors and rotation matrices into model weights, thereby minimizing the quantization overhead. During inference, we only perform online RHT for input activations of convolution layers, incurring only a 2.15% additional computational overhead.

3.3 Quantization-Distillation Low-Rank Adaptation

Under extremely low bit-width configurations, generative models face severe difficulty in producing viable outputs. Incorporating a high-precision branch to mitigate quantization errors is a widely adopted strategy [15, 21]. SVDQuant [15] shows that initializing these branches via singular value decomposition (SVD) [46] has proven to be particularly effective. Inspired by SVDQuant, we use a low-rank branch initialized by SVD to reduce the quantization error. This can be formulated as follows [15]:

$$XW = XL_1L_2 + XR \approx XL_1L_2 + Q(X)Q(R), \quad R = W - L_1L_2, \quad (9)$$

where the SVD of $W = U\Sigma V$, the r rank optimal solution is $L_1 = U\Sigma_{:,1:r}$, $L_2 = V_{r,:}$. However, most update rules for low-rank branches used in previous works are heuristic [15, 47], and do not guarantee convergence. Meanwhile, existing approaches predominantly concentrate on minimizing

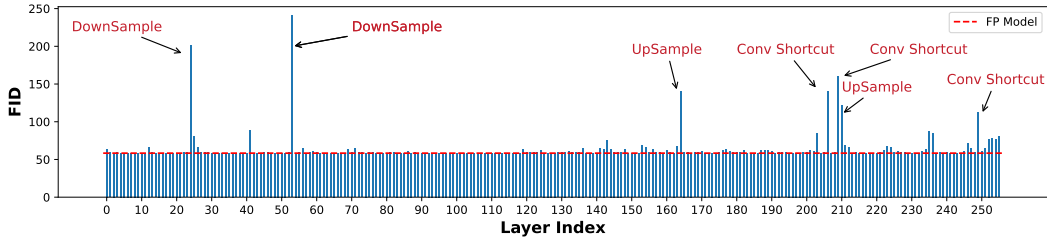


Figure 5: The change in FID on FFHQ when quantizing the activation of each layer individually at 4-bit precision. Different layers exhibit varying levels of sensitivity to quantization. Downsampling, upsampling, and residual connections are bottlenecks for quantization.

per-layer quantization error and often neglect the final results. Moreover, previous studies [48, 49] find that minimizing per-layer reconstruction error does not necessarily optimize the generation quality. We need a more suitable update scheme for the low-rank branches.

To solve this problem, a straightforward alternative is Low-Rank Adaptation (LoRA) [50], a Parameter-Efficient Fine-Tuning method, to align the quantized model with the FP model. However, although this approach is effective, the resulting image quality remains unsatisfactory. Inspired by FBquant [51], we confirmed that training the SVD-initialized low-rank branch would regularize the model to not deviate too far from the original one. But meanwhile, this strong constraint impedes distillation from the FP model to the quantized model. To remedy this problem, we introduce additional degrees of freedom into optimization. Therefore, we are able to conduct effective model fine-tuning.

Specifically, we propose Quantization-Distillation Low-Rank Adaptation (QD-LoRA). We train two low-rank branches simultaneously, while maintaining an identical number of parameters with SVDQuant [15]. The first branch is initialized via SVD and constrained by the backbone weights during training. It is designed to prevent excessive deviation from the original parameters. The second branch utilizes standard LoRA initialization and is dedicated to distilling knowledge from the FP model to the quantized one. The inference procedure is formulated as follows:

$$XW = XL_1L_2 + XR \approx XAB + XL_1L_2 + Q(X)Q(R), \quad R = W - L_1L_2, \quad (10)$$

where we use a random Gaussian initialization for A and zero for B . After training, the two low-rank branches can be merged together. That means the auxiliary low-rank branch does not introduce any additional computational overhead during inference, compared with SVDQuant [15].

In practice, we find that QD-LoRA achieves superior face restoration performance compared to optimizing a single low-rank branch while maintaining an identical number of parameters.

3.4 Adaptive Bit-width Allocation

Another challenge in low-bit quantization is the suboptimal allocation of limited resources. Previous works [20] notice that different layers exhibit varying sensitivities to quantization. We measure the change in FID [52] on FFHQ [53] by quantizing the activations of each layer individually, and we observe analogous findings in activation quantization. As illustrated in Fig. 5, within the OSDFace UNet, key convolution layers and residual connections have an outsized impact on the final image quality. After identifying the quantization bottlenecks, we can then devise a mixed-precision scheme. We assign a greater bit-width to those sensitive layers while keeping the resource budget unchanged.

Enlightened by prior works [54, 20, 55], we model the bit-width allocation as an integer programming problem, which is called adaptive bit-width allocation. The integer programming problem can be solved efficiently, compared with other methods like genetic algorithms [56].

When designing our integer programming objective, we focus on both reconstruction error and perception metric. Prior works [44, 20] observe that simply allocating higher bit-widths to layers with large reconstruction error (*i.e.*, MSE) does not guarantee better visual performance. Consequently, we employ a heuristic approach to assign perceptual error weight to each activation layer. Specifically, we first quantize the activation of every single layer to 2 bits, while keeping the remaining activation values in full precision. We then progressively increase the bit-width of the quantized activation until the FID difference compared to the FP model is within ϵ , or until the maximum bit-width B_{max} is reached. Then, for each layer i , we extract the corresponding bit-width B_i and assign the perceptual error weight as $w_i = 2^{B_i} - 1$. In practice, we set $\epsilon = 0.02$, $B_{max} = 8$.

Table 1: Quantitative comparison on the *synthetic dataset* CelebA-Test [57]. The best and second best results are colored with red and blue.

Bits (W/A)	Methods	CLIP-IQA \uparrow	DISTS \downarrow	LPIPS \downarrow	MANIQA \uparrow	MUSIQ \uparrow	NIQE \downarrow	Deg. \downarrow	LMD \downarrow	FID (FFHQ) \downarrow	FID (CelebA) \downarrow
32/32	OSDFace [12]	0.6910	0.1773	0.3365	0.5423	75.64	3.884	60.0708	5.287	45.41	17.06
6/6	MaxMin [38]	0.1781	0.4022	0.6082	0.1406	12.95	11.512	79.7129	11.214	234.94	216.67
	Q-Diffusion [17]	0.3679	0.2853	0.4784	0.1770	24.23	6.821	73.5904	7.840	81.43	75.69
	EfficientDM [21]	0.4571	0.2493	0.4128	0.3820	53.75	7.269	63.4590	5.800	63.47	34.77
	PassionSR [14]	0.6309	0.1762	0.3368	0.4731	72.74	4.125	61.5067	5.633	43.08	23.00
	SVDQuant [15]	0.6566	0.1774	0.3397	0.4818	73.59	4.021	60.7007	5.501	44.57	22.44
	QuantFace	0.6539	0.1740	0.3339	0.4893	74.43	4.045	60.1039	5.363	41.84	19.23
4/6	MaxMin [38]	0.1694	0.4144	0.6354	0.1472	12.93	12.864	80.8289	14.038	261.82	251.00
	Q-Diffusion [17]	0.2399	0.3541	0.5505	0.1141	16.45	9.091	77.0839	9.125	136.06	118.48
	EfficientDM [21]	0.4981	0.2475	0.4113	0.4119	55.96	7.212	64.8563	6.096	60.11	33.96
	PassionSR [14]	0.6391	0.1803	0.3401	0.4719	72.38	4.326	63.3448	5.737	45.73	26.01
	SVDQuant [15]	0.6912	0.1884	0.3639	0.4732	71.79	3.762	63.3879	6.043	50.51	33.18
	QuantFace	0.6510	0.1770	0.3442	0.4612	72.83	4.127	61.7154	5.658	42.18	23.36
4/4	MaxMin [38]	0.2045	0.4466	0.6867	0.2137	13.45	18.011	82.1358	16.783	315.62	311.01
	Q-Diffusion [17]	0.1747	0.4258	0.6660	0.1838	13.26	16.620	82.0933	17.066	295.58	289.39
	EfficientDM [21]	0.1992	0.4326	0.6368	0.1692	13.05	15.275	81.6171	15.463	265.51	254.24
	PassionSR [14]	0.3248	0.3426	0.5603	0.1398	15.66	6.821	82.4272	18.233	250.54	279.35
	SVDQuant [15]	0.5192	0.2563	0.4143	0.3572	58.90	5.709	76.3504	10.387	84.91	72.36
	QuantFace	0.6045	0.1867	0.3485	0.4255	71.49	4.813	67.5026	5.951	55.16	32.52
4/3.98	QuantFace-MP	0.5998	0.1830	0.3383	0.4491	73.00	4.708	65.7544	5.860	51.02	27.72

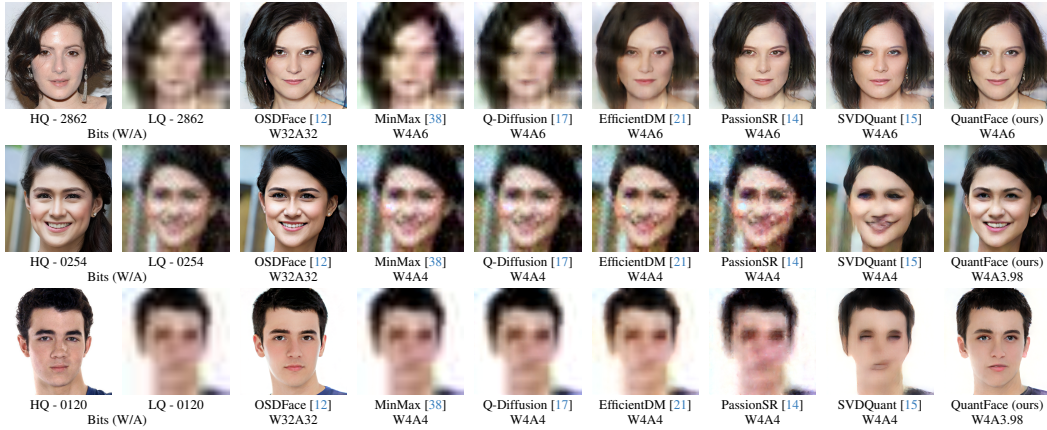


Figure 6: Visual comparison of the *synthetic* CelebA-Test dataset in challenging cases.

Given the total bits budget \mathcal{B} , and candidate bit-widths $b \in \{3, 4, 5, 6\}$, the quantization error of each layer is $\mathcal{L}_{i,b} = w_i^2 \|WX - Q(W)Q(X)\|_F^2$. After collecting the weighted quantization errors for each layer, the optimization problem can be solved in tens of seconds to a few minutes.

The Detailed integer programming workflow can be formulated as follows [54]:

$$\begin{aligned}
 & \underset{a_{i,b}}{\operatorname{argmin}} \quad \sum_{i=1}^N \sum_{b=3,4,5,6} a_{i,b} \cdot \mathcal{L}_{i,b} \\
 & \text{s.t.} \quad \sum_{b=3,4,5,6} a_{i,b} = 1, \quad \sum_{i=1}^N \sum_{b=3,4,5,6} a_{i,b} \cdot \mathcal{M}_{i,b} \leq \mathcal{B}, \\
 & \quad a_{i,b} \in \{0, 1\}, \quad \forall i \in \{1, \dots, N\}, \forall b \in \{3, 4, 5, 6\},
 \end{aligned} \tag{11}$$

where N is the number of layers, $a_{i,b} = 1$ denotes that the i -th layer will be quantized to b -bit, and $\mathcal{M}_{i,b}$ indicates the cost of the i -th layer when it is quantized to b -bit.

Under the overall W4A4 resource constraints, we applied the aforementioned integer programming approach to allocate appropriate bit-widths for activation quantization.

4 Experiments

4.1 Experiment Settings

Data Construction. We randomly select 512 high-quality face images from FFHQ [53] and resized them to 512×512 pixels. We obtained our synthetic training data using a dual-stage degradation model which is consistent with WaveFace [58]. The synthetic data collected in this manner closely aligns with the distribution of low-quality face images observed in real-world scenarios. we evaluate

Table 3: Quantitative comparison on *real-world datasets*. C-IQA stands for CLIPQA, and M-IQA stands for MANIQA. The best and second best results are colored with **red** and **blue**. MP stands for mixed-precision configuration generated by adaptive bit-width allocation.

Bits (W/A)	Methods	WebPhoto-Test [60]					LFW-Test [61]					Wider-Test [59]				
		C-IQA↑	M-IQA↑	MUSIQ↑	NIQE↓	FID↓	C-IQA↑	M-IQA↑	MUSIQ↑	NIQE↓	FID↓	C-IQA↑	M-IQA↑	MUSIQ↑	NIQE↓	FID↓
32/32	OSDFace [12]	0.7106	0.5162	73.94	3.986	84.60	0.7203	0.5493	75.35	3.871	44.63	0.7284	0.5229	74.60	3.774	34.65
	MaxMin [38]	0.2263	0.1291	24.68	7.816	137.31	0.2652	0.1927	39.63	6.753	118.28	0.2053	0.1062	15.67	9.418	152.62
	Q-Diffusion [17]	0.3775	0.2145	39.18	5.683	100.06	0.4743	0.2853	52.38	5.134	72.50	0.3741	0.1751	29.01	6.322	66.50
	EfficientDM [21]	0.5106	0.3570	56.85	5.665	100.04	0.5793	0.3980	62.62	4.818	68.69	0.5127	0.3643	52.52	6.325	49.09
	PassionSR [14]	0.6666	0.4535	70.37	4.304	82.02	0.6824	0.4849	72.94	3.988	47.90	0.6733	0.4594	70.93	4.145	39.32
	SVDQuant [15]	0.6927	0.4668	71.51	4.178	84.29	0.7024	0.4963	73.96	3.964	46.22	0.6841	0.4520	71.79	4.171	39.38
QuantFace	0.6939	0.4746	72.71	4.285	83.67	0.7055	0.4986	74.75	3.914	44.96	0.6981	0.4738	73.32	4.073	34.90	
4/6	MaxMin [38]	0.2204	0.1246	22.47	8.565	143.13	0.2538	0.1924	36.46	7.266	121.44	0.1978	0.1027	14.75	10.228	165.05
	Q-Diffusion [17]	0.2908	0.1568	28.86	6.841	116.86	0.3558	0.2193	42.46	6.027	94.05	0.2552	0.1132	19.27	7.918	104.15
	EfficientDM [21]	0.5840	0.4120	61.48	5.442	92.52	0.6166	0.4314	64.51	4.716	63.82	0.5479	0.3960	54.76	6.292	47.06
	PassionSR [14]	0.6578	0.4423	69.01	4.456	83.98	0.6485	0.4501	70.58	4.205	52.42	0.6623	0.4480	69.31	4.407	41.10
	SVDQuant [15]	0.6137	0.4294	70.62	4.597	83.95	0.6292	0.4368	71.78	4.334	49.95	0.6123	0.4288	70.38	4.608	41.45
	QuantFace	0.6841	0.4565	70.67	4.340	82.79	0.6965	0.4862	73.03	4.092	44.80	0.6667	0.4599	72.26	4.073	36.92
4/4	MaxMin [38]	0.2281	0.1600	18.89	11.055	167.46	0.2533	0.2019	28.03	9.356	141.90	0.2115	0.1497	14.20	12.837	194.46
	Q-Diffusion [17]	0.2158	0.1328	19.55	10.224	155.27	0.2417	0.1827	30.42	8.532	128.19	0.2010	0.1262	14.09	12.239	183.76
	EfficientDM [21]	0.2207	0.1128	21.43	8.996	161.68	0.2589	0.1228	32.36	6.779	129.42	0.2086	0.1234	14.81	11.494	172.48
	PassionSR [14]	0.3362	0.1667	27.39	6.059	204.05	0.3657	0.1857	36.75	6.649	151.02	0.3845	0.1747	20.18	6.419	270.94
	SVDQuant [15]	0.5647	0.3940	62.98	5.320	111.49	0.5741	0.3955	62.97	5.023	67.15	0.5383	0.3657	58.45	5.683	72.41
	QuantFace	0.6018	0.3978	67.57	5.043	95.01	0.5934	0.4029	67.78	4.619	52.79	0.6223	0.4152	68.57	5.039	42.34
4/3.98	QuantFace-MP	0.6453	0.4391	70.52	5.059	93.60	0.6372	0.4468	71.50	4.518	47.34	0.6375	0.4359	70.55	4.930	38.53

our quantized model on both synthetic and real-world datasets. The synthetic dataset is CelebA-Test [57] from DAEFR [27] and the real-world datasets are Wider-Test [59], WebPhoto-Test [60], and LFW-Test [61], which are consistent with OSDFace [12].

Metrics. For the *Synthetic Datasets*, LPIPS [62] and DISTs [63] are adopted as reference-based perceptual measures, together with CLIPQA [64], MANIQA [65], NIQE [66], and MUSIQ [67] as non-reference metrics. FID [52] with both FFHQ [53] and CelebA-Test HQ [57] are used to evaluate the distribution similarity between the real faces and generated ones. Moreover, following the previous face restoration works [24, 59, 27], we also evaluate the embedding angle of ArcFace [68] called ‘Deg.’, and the landmark distance named ‘LMD’. For the *Real-world Datasets*, CLIPQA [64], MANIQA [65], MUSIQ [67], NIQE [66], and FID [52] with FFHQ [53] are employed.

Implementation Details. Learning rate for QuantFace is set to 10^{-5} using the Adam [69] optimizer. Only the low-rank branches of each layer are updated during training, and the LoRA rank for both branches is 8. The loss function jointly integrates a perceptual loss in the pixel domain with a numerical reconstruction loss, which is formulated as:

$$\mathcal{L} = \lambda_1 \mathcal{L}_{\text{lpiips}}(I_q, I_{fp}) + \lambda_2 \mathcal{L}_{\text{mse}}(I_q, I_{fp}), \quad (12)$$

here, we set $\lambda_1 = 0.5$, $\lambda_2 = 0.5$ empirically. Experiments are conducted on a single NVIDIA A800 GPU, consuming 35.7 GB of GPU memory and 2.6 hours of GPU time.

Compard Methods. We compare QuantFace with several representative quantization methods: MaxMin [38], Q-Diffusion [17], EfficientDM [21], PassionSR [14], and SVDQuant [15]. Q-Diffusion [17], EfficientDM [21], and SVDQuant [15] are quantization methods for multi-step diffusion models. PassionSR [14] is a quantization method designed for one-step diffusion models.

Compression Ratio. To evaluate computational cost, following previous work [70], we measure the total model size (Params / M) and the number of operations (Ops / G). The results are summarized in Tab. 2. Under the 4-bit setting, our QuantFace achieves approximately 84.85% compression ratio for parameters and 82.91% compression ratio for computation.

Table 2: Params, Ops, and compression ratio of various settings. Ops are computed with input size 512×512 .

Method	Bits	Params / M (↓ Ratio)	Ops / G (↓ Ratio)
OSDFace [12]	W32A32	978 (↓0%)	4,264 (↓0%)
QuantFace	W6A6	209 (↓78.61%)	995 (↓76.66%)
	W4A6	148 (↓84.85%)	848 (↓80.10%)
	W4A4	148 (↓84.85%)	728 (↓82.91%)

4.2 Main Results

Quantitative Results. The results of the synthetic dataset are in Tab. 1 and the results of real-world datasets are in Tab. 3. These results indicate that QuantFace outperforms existing post-training quantization methods across most evaluation metrics under W4A4, W4A6, and W6A6 precision settings. Notably, at W4A4 precision, our approach surpasses the state-of-the-art method on every metric. Reference-based metrics such as LPIPS and DISTs indicate that QuantFace achieves smaller perceptual deviations from the ground-truth images, while lower LMD and Deg. further show that QuantFace restores the facial structure faithfully.

Table 4: Ablation studies on different components. Experiments are conducted on the *synthetic dataset* CelebA-Test [57] and the bit setting is W4A4. The best and the second best results are colored **red** and **blue**, respectively. Rotation stands for rotation-scaling channel balancing, and MP stands for mixed-precision configuration generated by adaptive bit-width allocation.

Rotation	QD-LoRA	MP	CLIP-IQA \uparrow	DISTS \downarrow	LPIPS \downarrow	MANIQA \uparrow	MUSIQ \uparrow	NIQE \downarrow	Deg. \downarrow	LMD \downarrow	FID (FFHQ) \downarrow	FID (CelebA) \downarrow
			0.5192	0.2563	0.4143	0.3572	58.90	5.709	76.3504	10.387	84.91	72.36
✓			0.6391	0.2059	0.3651	0.4897	72.22	4.739	70.7017	6.701	62.56	44.11
	✓		0.5510	0.2210	0.3777	0.3773	65.17	5.390	72.7748	7.418	61.52	47.37
		✓	0.5879	0.2124	0.3703	0.4193	69.44	4.955	72.2776	7.056	64.10	47.42
✓	✓		0.6045	0.1867	0.3485	0.4255	71.49	4.813	67.5026	5.951	55.16	32.52
		✓	0.5975	0.2078	0.3631	0.4272	71.29	4.955	72.0443	7.047	57.68	43.68
✓	✓	✓	0.5996	0.1959	0.3503	0.4363	68.94	4.761	66.3513	6.043	52.77	37.75
✓	✓	✓	0.5998	0.1830	0.3383	0.4491	73.00	4.708	65.7544	5.860	51.02	27.72

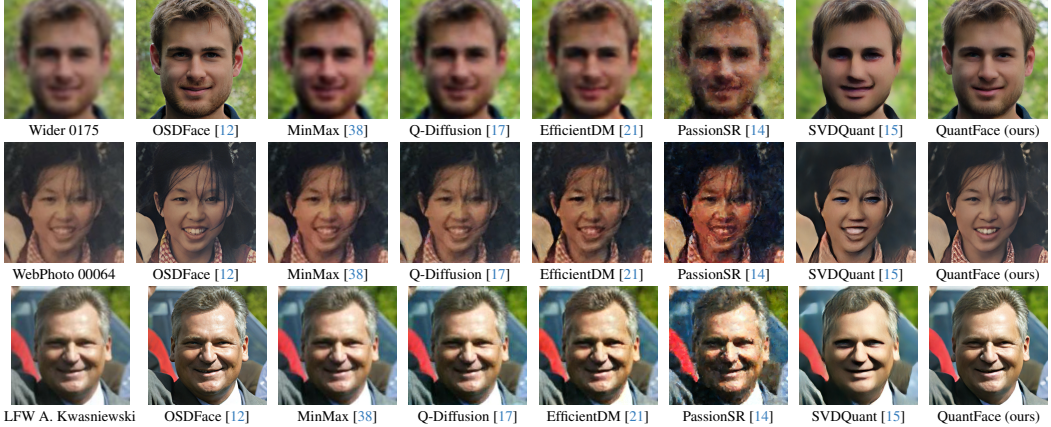


Figure 7: Visual performance comparison on *real-world datasets*. Please zoom in for a better view. Our QuantFace is under bit-width W4A3.98 and other methods are under W4A4.

Quality Results. We show the visual comparison results of the synthetic datasets in Fig. 6 and real-world datasets in Fig. 7. Our method reconstructs a wide range of facial details effectively, such as eyes, hair, and other elements that are prone to distortion after quantization. Moreover, even under 4-bit precision, our method still generates high-fidelity face images compared with others.

4.3 Ablation Studies

Rotation-Scaling Channel Balancing. As illustrated in Fig. 4, solely applying scaling leads to uneven data distribution across channels, making it challenging to preserve the original data distribution after quantization. On the other hand, using the Randomized Hadamard Transform (RHT) alone fails to eliminate extreme outliers in the activations. By combining both techniques, we can effectively maintain the data distribution while reducing quantization errors. Consequently, we are able to enhance the final face restoration performance.

Quantization-Distillation Low-Rank Adaptation. The results presented in the Tab. 4 demonstrate that QD-LoRA effectively maintains a balance between quantization and distillation. QD-LoRA neither struggles to align with the FP model nor overfits to the limited calibration dataset. Therefore, models can generate excellent human face images after quantization. Results in Tab. 4 also reveal that QD-LoRA surpasses direct optimization on the SVD initialized low-rank branch.

Adaptive Bit-width Allocation. Various results shown in Tab. 1 and Tab. 4 demonstrate that our mixed-precision configuration enhances reference-based metrics on the synthetic dataset. The results indicate that the generated face images align closely with real-world face images. Visually, our configuration significantly improves the detail of generated facial features, including eyes and teeth.

5 Conclusion

We introduce QuantFace, an effective quantization framework for one-step diffusion face restoration models. QuantFace not only reduces quantization error but also facilitates the distillation from the full-precision model to the quantized model. Moreover, QuantFace promotes reasonable resource allocation. Extensive experiments demonstrate that QuantFace outperforms existing SOTA methods across a variety of metrics. By maintaining a balance between computational overhead and restoration quality, QuantFace makes the efficient deployment of advanced face restoration models possible.

References

- [1] I. J. Goodfellow, J. Pouget-Abadie, M. Mirza, B. Xu, D. Warde-Farley, S. Ozair, A. Courville, and Y. Bengio, “Generative adversarial nets,” *NeurIPS*, 2014. 1, 3
- [2] J. Ho, A. Jain, and P. Abbeel, “Denoising diffusion probabilistic models,” in *NeurIPS*, 2020. 1, 3
- [3] J. Song, C. Meng, and S. Ermon, “Denoising diffusion implicit models,” in *ICLR*, 2021. 1, 3
- [4] Y. Song, J. Sohl-Dickstein, D. P. Kingma, A. Kumar, S. Ermon, and B. Poole, “Score-based generative modeling through stochastic differential equations,” in *ICLR*, 2021. 1
- [5] B. Kawar, M. Elad, S. Ermon, and J. Song, “Denoising diffusion restoration models,” 2022. 1, 3
- [6] Y. Wang, J. Yu, and J. Zhang, “Zero-shot image restoration using denoising diffusion null-space model,” in *ICLR*, 2023. 1, 3
- [7] B. Fei, Z. Lyu, L. Pan, J. Zhang, W. Yang, T. Luo, B. Zhang, and B. Dai, “Generative diffusion prior for unified image restoration and enhancement,” in *CVPR*, 2023. 1, 3
- [8] P. Yang, S. Zhou, Q. Tao, and C. C. Loy, “PGDiff: Guiding diffusion models for versatile face restoration via partial guidance,” 2023. 1, 3
- [9] T. Yin, M. Gharbi, R. Zhang, E. Shechtman, F. Durand, W. T. Freeman, and T. Park, “One-step diffusion with distribution matching distillation,” in *CVPR*, 2024. 1, 4
- [10] Y. Song, P. Dhariwal, M. Chen, and I. Sutskever, “Consistency models,” 2023. 1
- [11] J. Li, J. Cao, Z. Zou, X. Su, X. Yuan, Y. Zhang, Y. Guo, and X. Yang, “Distillation-free one-step diffusion for real-world image super-resolution,” *arXiv preprint arXiv:2410.04224*, 2024. 1
- [12] J. Wang, J. Gong, L. Zhang, Z. Chen, X. Liu, H. Gu, Y. Liu, Y. Zhang, and X. Yang, “Osdface: One-step diffusion model for face restoration,” *arXiv preprint arXiv:2411.17163*, 2024. 1, 2, 5, 7, 8, 9
- [13] X. Lin, J. He, Z. Chen, Z. Lyu, B. Dai, F. Yu, Y. Qiao, W. Ouyang, and C. Dong, “Diffbir: Toward blind image restoration with generative diffusion prior,” in *ECCV*, 2024. 2
- [14] L. Zhu, J. Li, H. Qin, W. Li, Y. Zhang, Y. Guo, and X. Yang, “Passionsr: Post-training quantization with adaptive scale in one-step diffusion based image super-resolution,” *arXiv preprint arXiv:2411.17106*, 2024. 2, 3, 7, 8, 9
- [15] M. Li, Y. Lin, Z. Zhang, T. Cai, J. Guo, X. Li, E. Xie, C. Meng, J.-Y. Zhu, and S. Han, “SVDQuant: Absorbing outliers by low-rank component for 4-bit diffusion models,” in *ICLR*, 2025. 2, 3, 4, 5, 6, 7, 8, 9
- [16] M. Nagel, M. Fournarakis, R. A. Amjad, Y. Bondarenko, M. Van Baalen, and T. Blankevoort, “A white paper on neural network quantization,” *arXiv preprint arXiv:2106.08295*, 2021. 1, 4
- [17] X. Li, Y. Liu, L. Lian, H. Yang, Z. Dong, D. Kang, S. Zhang, and K. Keutzer, “Q-diffusion: Quantizing diffusion models,” in *ICCV*, 2023. 2, 7, 8, 9
- [18] Y. He, L. Liu, J. Liu, W. Wu, H. Zhou, and B. Zhuang, “Ptqd: Accurate post-training quantization for diffusion models,” in *NeurIPS*, 2023. 2, 3
- [19] Y. Shang, Z. Yuan, B. Xie, B. Wu, and Y. Yan, “Post-training quantization on diffusion models,” in *CVPR*, 2023. 2, 3
- [20] Y. Sui, Y. Li, A. Kag, Y. Idelbayev, J. Cao, J. Hu, D. Sagar, B. Yuan, S. Tulyakov, and J. Ren, “Bitsfusion: 1.99 bits weight quantization of diffusion model,” in *NeurIPS*, 2024. 2, 6
- [21] Y. He, J. Liu, W. Wu, H. Zhou, and B. Zhuang, “Efficientdm: Efficient quantization-aware fine-tuning of low-bit diffusion models,” in *ICLR*, 2024. 2, 3, 5, 7, 8, 9

- [22] G. Xiao, J. Lin, M. Seznec, H. Wu, J. Demouth, and S. Han, “Smoothquant: Accurate and efficient post-training quantization for large language models,” in *ICML*, 2023. 2, 3, 4
- [23] R. Rombach, A. Blattmann, D. Lorenz, P. Esser, and B. Ommer, “High-resolution image synthesis with latent diffusion models,” in *CVPR*, 2022. 3
- [24] Y. Gu, X. Wang, L. Xie, C. Dong, G. Li, Y. Shan, and M.-M. Cheng, “Vqfr: Blind face restoration with vector-quantized dictionary and parallel decoder,” in *ECCV*, 2022. 3, 8
- [25] S. Zhou, K. C. Chan, C. Li, and C. C. Loy, “Towards robust blind face restoration with codebook lookup transformer,” 2022. 3
- [26] Z. Wang, J. Zhang, T. Chen, W. Wang, and P. Luo, “Restoreformer++: Towards real-world blind face restoration from undegraded key-value pairs,” *IEEE TPAMI*, 2023. 3
- [27] Y.-J. Tsai, Y.-L. Liu, L. Qi, K. C. Chan, and M.-H. Yang, “Dual associated encoder for face restoration,” *arXiv preprint arXiv:2308.07314*, 2023. 3, 8
- [28] Z. Yao, R. Yazdani Aminabadi, M. Zhang, X. Wu, C. Li, and Y. He, “Zeroquant: Efficient and affordable post-training quantization for large-scale transformers,” in *NeurIPS*, 2022. 3
- [29] Y. Li, R. Gong, X. Tan, Y. Yang, P. Hu, Q. Zhang, F. Yu, W. Wang, and S. Gu, “Brecq: Pushing the limit of post-training quantization by block reconstruction,” in *ICLR*, 2021. 3
- [30] Y. Bhalgat, J. Lee, M. Nagel, T. Blankevoort, and N. Kwak, “Lsq+: Improving low-bit quantization through learnable offsets and better initialization,” in *CVPR*, 2020. 3
- [31] M. Chen, W. Shao, P. Xu, J. Wang, P. Gao, K. Zhang, Y. Qiao, and P. Luo, “Efficientqat: Efficient quantization-aware training for large language models,” *arXiv preprint arXiv:2407.11062*, 2024. 3
- [32] C. Yu, S. Yang, F. Zhang, H. Ma, A. Wang, and E.-P. Li, “Improving quantization-aware training of low-precision network via block replacement on full-precision counterpart,” *arXiv preprint arXiv:2412.15846*, 2024. 3
- [33] Z. Liu, B. Oguz, C. Zhao, E. Chang, P. Stock, Y. Mehdad, Y. Shi, R. Krishnamoorthi, and V. Chandra, “Llm-qat: Data-free quantization aware training for large language models,” in *ACL*, 2024. 3
- [34] Y. Bondarenko, R. Del Chiaro, and M. Nagel, “Low-rank quantization-aware training for llms,” *arXiv preprint arXiv:2406.06385*, 2024. 3
- [35] Y. Li, Y. Yu, C. Liang, P. He, N. Karampatziakis, W. Chen, and T. Zhao, “Loftq: Lora-fine-tuning-aware quantization for large language models,” in *ICLR*, 2023. 3
- [36] X. Li, Y. Liu, L. Lian, H. Yang, Z. Dong, D. Kang, S. Zhang, and K. Keutzer, “Q-diffusion: Quantizing diffusion models,” in *ICCV*, 2023. 3
- [37] Y. Li, S. Xu, X. Cao, X. Sun, and B. Zhang, “Q-dm: An efficient low-bit quantized diffusion model,” in *NeurIPS*, 2024. 3
- [38] B. Jacob, S. Kligys, B. Chen, M. Zhu, M. Tang, A. Howard, H. Adam, and D. Kalenichenko, “Quantization and training of neural networks for efficient integer-arithmetic-only inference,” in *CVPR*, 2018. 4, 7, 8, 9
- [39] Z. Liu, K.-T. Cheng, D. Huang, E. Xing, and Z. Shen, “Nonuniform-to-uniform quantization: Towards accurate quantization via generalized straight-through estimation,” in *CVPR*, 2022. 4
- [40] O. Ronneberger, P. Fischer, and T. Brox, “U-net: Convolutional networks for biomedical image segmentation,” in *MICCAI*, 2015. 4, 5
- [41] A. Tseng, J. Chee, Q. Sun, V. Kuleshov, and C. De Sa, “Quip#: Even better llm quantization with hadamard incoherence and lattice codebooks,” *arXiv preprint arXiv:2402.04396*, 2024. 4, 5

- [42] S. Ashkboos, A. Mohtashami, M. Croci, B. Li, P. Cameron, M. Jaggi, D. Alistarh, T. Hoefler, and J. Hensman, “Quarot: Outlier-free 4-bit inference in rotated llms,” *NeurIPS*, 2024. 4, 5
- [43] Z. Liu, C. Zhao, I. Fedorov, B. Soran, D. Choudhary, R. Krishnamoorthi, V. Chandra, Y. Tian, and T. Blankevoort, “Spinquant: Llm quantization with learned rotations,” *arXiv preprint arXiv:2405.16406*, 2024. 4
- [44] T. Zhao, T. Fang, H. Huang, E. Liu, R. Wan, W. Soedarmadji, S. Li, Z. Lin, G. Dai, S. Yan, *et al.*, “Vidit-q: Efficient and accurate quantization of diffusion transformers for image and video generation,” *arXiv preprint arXiv:2406.02540*, 2024. 4, 6
- [45] Z. Xu, Y. Yue, X. Hu, Z. Yuan, Z. Jiang, Z. Chen, J. Yu, C. Xu, S. Zhou, and D. Yang, “Mambaquant: Quantizing the mamba family with variance aligned rotation methods,” *arXiv preprint arXiv:2501.13484*, 2025. 5
- [46] C. Eckart and G. Young, “The approximation of one matrix by another of lower rank,” *Psychometrika*, 1936. 5
- [47] H. Guo, P. Greengard, E. Xing, and Y. Kim, “Lq-lora: Low-rank plus quantized matrix decomposition for efficient language model finetuning,” *ICLR*, 2024. 5
- [48] C. Zhang, J. T. Wong, C. Xiao, G. A. Constantinides, and Y. Zhao, “Qera: an analytical framework for quantization error reconstruction,” *ICLR*, 2025. 6
- [49] Z. Deng, X. Wang, S. Sharify, and M. Orshansky, “Mixed-precision quantization with cross-layer dependencies,” *arXiv preprint arXiv:2307.05657*, 2023. 6
- [50] E. J. Hu, Y. Shen, P. Wallis, Z. Allen-Zhu, Y. Li, S. Wang, L. Wang, W. Chen, *et al.*, “Lora: Low-rank adaptation of large language models,” *ICLR*, 2022. 6
- [51] Y. Liu, H. Fang, L. He, R. Zhang, Y. Bai, Y. Du, and L. Du, “Fbquant: Feedback quantization for large language models,” *arXiv preprint arXiv:2501.16385*, 2025. 6
- [52] M. Heusel, H. Ramsauer, T. Unterthiner, B. Nessler, and S. Hochreiter, “Gans trained by a two time-scale update rule converge to a local nash equilibrium,” in *NeurIPS*, 2017. 6, 8
- [53] T. Karras, S. Laine, and T. Aila, “A style-based generator architecture for generative adversarial networks,” in *CVPR*, 2019. 6, 7, 8
- [54] T. Zhao, X. Ning, T. Fang, E. Liu, G. Huang, Z. Lin, S. Yan, G. Dai, and Y. Wang, “Mixdq: Memory-efficient few-step text-to-image diffusion models with metric-decoupled mixed precision quantization,” in *ECCV*, 2024. 6, 7
- [55] Y. Ma, T. Jin, X. Zheng, Y. Wang, H. Li, Y. Wu, G. Jiang, W. Zhang, and R. Ji, “Ompq: Orthogonal mixed precision quantization,” in *AAAI*, 2023. 6
- [56] L. Chen, Y. Meng, C. Tang, X. Ma, J. Jiang, X. Wang, Z. Wang, and W. Zhu, “Q-dit: Accurate post-training quantization for diffusion transformers,” *arXiv preprint arXiv:2406.17343*, 2024. 6
- [57] T. Karras, T. Aila, S. Laine, and J. Lehtinen, “Progressive growing of gans for improved quality, stability, and variation,” *arXiv preprint arXiv:1710.10196*, 2017. 7, 8, 9
- [58] Y. Miao, J. Deng, and J. Han, “Waveface: Authentic face restoration with efficient frequency recovery,” in *CVPR*, 2024. 7
- [59] S. Zhou, K. Chan, C. Li, and C. C. Loy, “Towards robust blind face restoration with codebook lookup transformer,” *NeurIPS*, 2022. 8
- [60] X. Wang, Y. Li, H. Zhang, and Y. Shan, “Towards real-world blind face restoration with generative facial prior,” in *CVPR*, 2021. 8
- [61] G. B. Huang, M. Mattar, T. Berg, and E. Learned-Miller, “Labeled Faces in the Wild: A Database for Studying Face Recognition in Unconstrained Environments,” in *Workshop on Faces in ‘Real-Life’ Images: Detection, Alignment, and Recognition*, 2008. 8

- [62] R. Zhang, P. Isola, A. A. Efros, E. Shechtman, and O. Wang, “The unreasonable effectiveness of deep features as a perceptual metric,” in *CVPR*, 2018. 8
- [63] K. Ding, K. Ma, S. Wang, and E. P. Simoncelli, “Image quality assessment: Unifying structure and texture similarity,” *PAMI*, 2020. 8
- [64] J. Wang, K. C. Chan, and C. C. Loy, “Exploring clip for assessing the look and feel of images,” in *AAAI*, 2023. 8
- [65] S. Yang, T. Wu, S. Shi, S. Lao, Y. Gong, M. Cao, J. Wang, and Y. Yang, “Maniqa: Multi-dimension attention network for no-reference image quality assessment,” in *CVPRW*, 2022. 8
- [66] L. Zhang, L. Zhang, and A. C. Bovik, “A feature-enriched completely blind image quality evaluator,” *TIP*, 2015. 8
- [67] J. Ke, Q. Wang, Y. Wang, P. Milanfar, and F. Yang, “MUSIQ: Multi-scale Image Quality Transformer,” in *ICCV*, 2021. 8
- [68] J. Deng, J. Guo, N. Xue, and S. Zafeiriou, “Arcface: Additive angular margin loss for deep face recognition,” in *CVPR*, 2019. 8
- [69] D. P. Kingma and J. Ba, “Adam: A method for stochastic optimization,” in *ICLR*, 2015. 8
- [70] H. Qin, Y. Zhang, Y. Ding, X. Liu, M. Danelljan, F. Yu, *et al.*, “Quantsr: accurate low-bit quantization for efficient image super-resolution,” *NeurIPS*, 2023. 8